

The role of phase in molecular Rydberg wave packet dynamics

R. A. L. Smith, V. G. Stavros, J. R. R. Verlet, and H. H. Fielding^{a)}

Department of Chemistry, King's College London, Strand, London WC2R 2LS, United Kingdom

D. Townsend and T. P. Softley

Physical and Theoretical Chemistry Laboratory, South Parks Road, Oxford OX1 3QZ, United Kingdom

(Received 14 January 2003; accepted 13 May 2003)

The dynamics of Rydberg wave packets in NO are investigated in the regime where the electronic period is comparable with the rotational motion of the molecular ion core. The presence of a rotating molecular core manifests itself in the wave packet dynamics as a series of peaks separated by the rotational beat period T_{Rot} , but offset by $\Delta\mu T_{\text{Rot}}$, where $\Delta\mu$ is the difference in quantum defect between the two dominant Rydberg series in the superposition. We rationalize this by treating the dynamics of a wave packet created from a coherent superposition of two interleaved Rydberg series as two separate electron wave packets, which interfere with one another when they overlap spatially. There is a periodic phase difference between the two wave packets that depends on the rotational energy of the core in each Rydberg series and also on the quantum defects. The resulting interference pattern in the Rydberg population manifests itself as peaks in the wave packet spectrum at the stroboscopic period. © 2003 American Institute of Physics. [DOI: 10.1063/1.1589473]

I. INTRODUCTION

The investigation of Rydberg electron wave packets is of practical importance because it represents the boundary between quantum and classical mechanics. An *atomic* electron wave packet, excited using the broad bandwidth of a short laser pulse, starts off reasonably well localized in the core region, then moves to the outer turning point of the Coulomb potential returning to core region periodically. The period of motion is $t_{cl} = 2\pi\bar{n}^3$, where \bar{n} is the “average” principal quantum number in the superposition and essentially provides a measure of the binding energy of the wave packet, $\bar{n} = (-2\epsilon)^{-1/2}$.^{1–5} This classical behavior breaks down at longer times as the quantum-mechanical nature of the wave packet manifests itself. The anharmonicity of the Coulomb potential causes the wave packet to disperse^{6–10} and produce interesting interference patterns called partial revivals. At longer times the situation is reversed and something resembling the initial wave packet forms again. The time at which this occurs is referred to as the revival time, T_R . This oscillation between classical- and quantum-mechanical behavior continues, in principle, until the Rydberg population is depleted via relevant decay mechanisms.

Our work on electron wave packets in molecules^{11–13} reveals a more complex picture. We have observed plateaus in plots of the period of motion of a molecular Rydberg wave packet as a function of the average principal quantum number in the superposition. These plateaus are present at times that, at first sight, correspond to the classical periods of rotation of the molecular ion core. Figure 1 represents an example in which wave packets were excited to Rydberg series converging to the ionization limits of the $X^1\Sigma^+$ state of NO^+ , via the $A^2\Sigma^+(v'=1, N'=0, J'=1/2)$ level of NO.

Selection rules predict that wave packets with predomi-

nantly $np(0)$ character would be excited, using the nomenclature $nl(N^+)$, where N^+ is the rotational quantum number of the molecular ion core. If this were the case the measured period of the wave packet would be expected to follow the hydrogenic curve plotted in Fig. 1 and labeled $t_{cl}(N^+=0)$. Due to the mixed angular momentum character of the A state, $np(2)$ and $nf(2)$ Rydberg series are also included in the superposition, and so it is useful to mark the hydrogenic curve for a wave packet composed of Rydberg states converging to the $N^+=2$ ionization limit, labeled $t_{cl}(N^+=2)$. The filled circles mark the dominant peaks in the experimental time-resolved spectra and the hollow circles mark distinct but less intense peaks. The dynamics do not follow either of the hydrogenic curves, but instead there are two very clear plateaus. The classical rotation period of the NO^+ core with $N^+=2$ is 3.46 ps, calculated (in atomic units) using

$$T_{N^+} = \frac{\pi}{B_{v^+} \sqrt{N^+(N^++1)}}, \quad (1)$$

where $B_1 = 1.969 \text{ cm}^{-1}$. Horizontal dotted lines in Fig. 1 mark the classical rotation period and twice the rotational period, and are in reasonable agreement with the experimentally measured recurrence times, implying that the dynamics of the Rydberg wave packet are influenced by the rotating molecular ion core. Figure 2 represents a portion of the same data but as a contour plot, which is obtained by recording many spectra. This figure shows how the whole shape of the recurrence spectrum evolves with excitation energy. At the point where the classical electronic period coincides with the rotational period there is a marked change in the appearance of the first recurrence peak. For $\bar{n}_0 < 29$ [where \bar{n}_{N^+} is the average principal quantum number measured in series $nl(N^+)$], almost hydrogenic behavior is observed and peaks are observed in the recurrence spectra at approximately the

^{a)} Author to whom correspondence should be addressed.

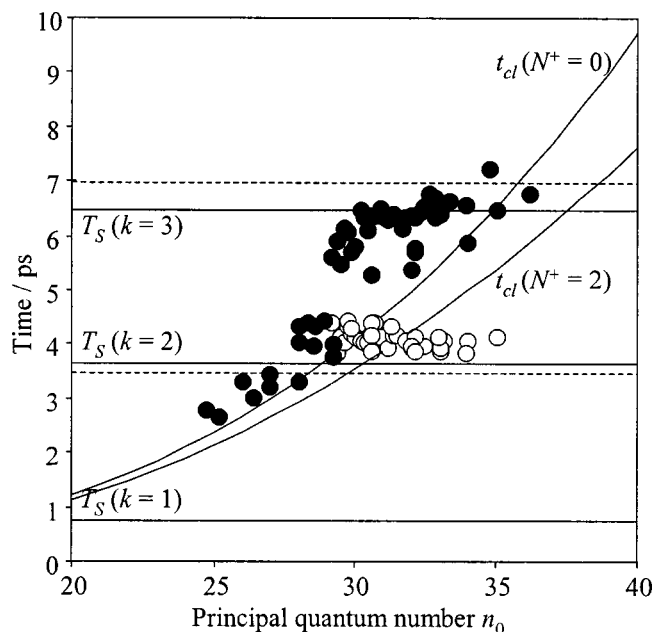


FIG. 1. A plot of the measured orbit period (filled circles=most intense peak; open circle=less intense but still prominent peak) as a function of average excitation energy expressed in terms of the average principal quantum number \bar{n}_0 , in the superposition. The wave packets are composed predominantly of $np(0)$ and $nf(2)$ Rydberg states with $\nu^+=1$. Trend lines mark the hydrogenic orbit periods $t_{cl}=2\pi\bar{n}^3$; dashed horizontal lines mark the classical rotation period of a molecular core with $N^+=2$, defined by Eq. (1); and solid horizontal lines mark the stroboscopic periods defined by Eq. (5).

classical orbit period, i.e., the electronic motion is dominant. For $\bar{n}_0 > 29$ the observed period no longer scales as \bar{n}^3 but forms plateaus, and the first peak in the recurrence spectrum is not necessarily the most intense. Clearly there is a strong coupling between the electronic and nuclear motion, which is the quantum-mechanical analog of mechanical resonance.

Molecular Rydberg states have been observed in the frequency domain in the regime where electronic and rotational periods are comparable. The first detailed analysis was by Martin *et al.*¹⁴ in 1983, who carried out a detailed spectro-

scopic analysis of the high Rydberg states of Na_2 , excited via resolved rovibrational levels of the $A^1\Sigma_u^+$ and $B^1\Pi_u$ states. The most interesting observations were made in spectra recorded via the $A^1\Sigma_u^+$ intermediate. Three Rydberg series were observed: the $nd^1\Pi_g$, $nd^1\Sigma_g^+$, and $ns^1\Sigma_g^+$ series. The two d series dominated the spectrum, and for high n a Hund's case (d) description is appropriate and they can be labeled $nd(N^+=J'+1)$ and $nd(N^+=J'-1)$. In regions of the spectrum where $nd(J'-1)$ and $(n-m)d(J'+1)$ Rydberg states lie close in energy (where m is an integer), the levels interacted strongly so that both were shifted and their eigenfunctions were mixed. This mixing of the eigenfunctions produced interference effects in the electric dipole probability so that only one of a pair of interacting lines remained intense, resulting in a simplification of the Rydberg spectrum. Such fringe patterns were observed in various regions of the spectrum and referred to as the stroboscopic effect. The positions of the fringes are obviously dependent on J' , which determines the difference between the ionization limits of the two series: $\Delta E_{\text{Rot}} = 4B_v^+(J'+1/2)$.

Subsequent papers by various authors^{15–20} have examined the relationship between the positions of the fringes and the principal quantum number. The general argument has been that in a homonuclear diatomic molecule, fringes are generated when the classical electronic period is an integer multiple of half the rotation period of the molecular ion core, i.e., $t_{cl} = kT_{\text{Rot}}/2$ or $k\omega_{cl} = 2\omega_{\text{Rot}}$. Since the internuclear axis appears at rest when the electron returns to the core, the projection of the orbital angular momentum onto the axis, Λ , is a good quantum number and a Hund's case (a) coupling scheme is appropriate. It is this behavior that gives the stroboscopic effect its name. The Rydberg electron is said to “light the core like a stroboscope with frequency ω_{cl} .”¹⁶ Using this definition, and the classical frequencies of electronic motion, $\omega_{cl} = n^{-3}$, and nuclear rotation, $\omega_{N^+} = 2B_v^+(J'+1/2)$, the stroboscopic effect occurs when

$$\nu^3 = \frac{k}{4B_v^+(J'+1/2)}. \quad (2)$$

It should be noted that Eq. (2) could be rearranged to give $\nu^3 = k/\Delta E_{\text{Rot}} \equiv k/2\omega_{N^+}$, which ties in with the coupling between electronic and molecular motion observed in our wave packet spectra. This definition of the stroboscopic effect assumes that there is one average electronic period and one average rotational period. In the limit of very high quantum numbers this is a reasonable approximation, but in reality molecular Rydberg states are still quantum systems, and therefore electronic and molecular phases play an important role in determining their dynamics, and so this description as it stands is incomplete.

Altunata *et al.* have included phase to some degree in a semiclassical model of electron wave packets in a homonuclear diatomic molecule, in which they employ a sum over classical trajectories method.²¹ The measurable quantity in these calculations is the autocorrelation function of the system, which can be considered as a probe of the state of the system. For the rotation of the core, the autocorrelation function is expressed as a sum over planar rotations, in the limit of high angular momentum quantum number, J , where the

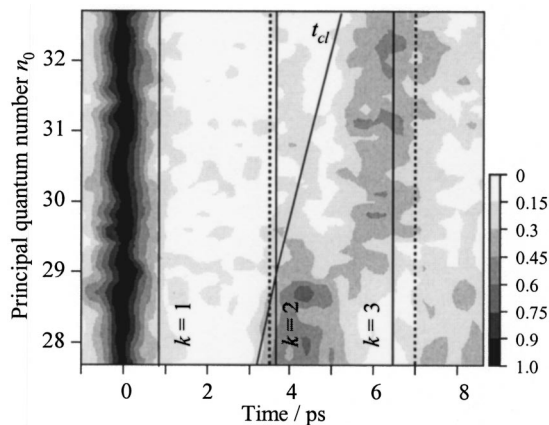


FIG. 2. A contour plot obtained by recording many spectra of wave packets excited via the $A^2\Sigma^+(v'=1, N'=0, J'=1/2)$ level of NO. This figure shows how the whole shape of the recurrence spectrum evolves with excitation energy. The rotational period is marked as a dashed line and the stroboscopic period (see the text) as a solid line.

semiclassical treatment is more accurate. During the rotation of the core, the nuclei interact with the Rydberg electron through long-range interactions. This aspect is modeled by describing the electronic motion inside a rotating frame with circular frequency equal to the rotation frequency of the core. The specific example presented employed quantum numbers $J=50$, $\bar{n}=8$, and molecular parameters to achieve the resonance condition $t_{cl}=2T_{\text{Rot}}$. Peaks are observed at times which are multiples of the classical electronic period, since integer multiples of the electronic period are even integer multiples of the rotational period, and both motions are therefore in phase. Dips in the spectra are observed at times corresponding to $(k \pm 0.25)t_{cl}$ when the nuclei have undergone $(2k \pm 0.5)$ periods, and therefore are in the opposite orientation than when the electron started. These minima arise from destructive interference between the wave functions that describe the two motions. On the other hand, when the electron has undergone half a classical period the nuclei have undergone a full rotation and constructive interference between the two wave functions results in a peak in the autocorrelation function.

In this paper, we present a detailed investigation of the dynamics of molecular Rydberg wave packets in the regime where the period of electronic motion is comparable to the nuclear rotation. Wave packet experiments are ideal for this problem since they give us a physical picture directly, but at the same time all the phase information is available. We approach our interpretation of the problem of resonances between electronic and nuclear motion from a different perspective than previous frequency and semiclassical pictures. We view the dynamics of a wave packet created from a coherent superposition of two interleaved Rydberg series with different rotational states of the molecular core, as two separate electron wave packets, which interfere with one another. We show that the resulting interference pattern can be explained in terms of the relative phases of the two wave packets, whose origins lie in the quantum defects of the Rydberg series and the rotation of the molecular core.

II. EXPERIMENT

A Continuum Nd:YAG laser produces 450 mJ in a 6 ns pulse of 532 nm radiation at 20 Hz. Twenty percent of this radiation is used to pump a Continuum tunable dye laser to produce red light around 615 nm. The tripled output of this dye laser is used to excite the $A^2\Sigma^+(v',N',J') \leftarrow X^2\Pi_{3/2}$ transition in NO. A mode-locked picosecond Nd:YAG laser produces 2 W of 532 nm radiation with a repetition rate of 76 MHz and pulse width of approximately 70 ps. This synchronously pumps a picosecond dye laser, which has a bandwidth of around $35 \pm 5 \text{ cm}^{-1}$ FWHM, and an average power of 220 mW. The dye laser output is manually tunable, and is scanned around 662 nm. This output is amplified in a series of Bethune cells and the amplified picosecond light is frequency doubled to around 331 nm (20 μJ per pulse). The doubled light enters a stabilized Michelson interferometer to generate a pair of pulses of equal intensity. One of the arms of the interferometer has a fixed path length. The other has a variable path length, allowing a variable delay to be introduced between the picosecond pulses. The doubled picosec-

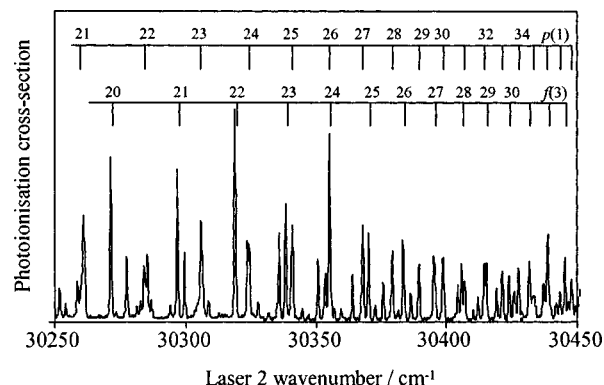


FIG. 3. A Rydberg spectrum of NO following excitation via the $A^2\Sigma^+(v'=2, N'=1, J'=3/2)$ intermediate in NO. The two most intense Rydberg series are $np(1)$ and $nf(3)$, and their unperturbed positions are calculated using the Rydberg formula using experimentally measured quantum defects $\mu_{p(1)}=0.7038$ and $\mu_{f(3)}=0.021$ (Ref. 26), and marked with combs.

ond radiation is used to excite from the $A^2\Sigma^+(v',N',J')$ intermediate level to Rydberg series converging to the $X^1\Sigma^+$ ionization limits of NO^+ . The wave packet dynamics are monitored using the optical Ramsey method.²² Briefly, the two pulses generated by the interferometer are used to create two identical Rydberg wave packets. Strong modulations in the final Rydberg population are observed as a function of the precise time between the pair of picosecond pulses, and the total population of Rydberg states is measured by pulsed field ionization. Wave packet spectra are obtained by plotting the root-mean-square of a least-squares fit to the ion signal fringes as a function of time, i.e., the autocorrelation function $\langle \Psi(t) | \Psi(0) \rangle$.

Complementary $1+1'$ REMPI frequency spectra were recorded using the Oxford Rydberg spectroscopy laser system.²³

III. RESULTS AND DISCUSSION

From previously reported frequency-resolved investigations of the Rydberg states of NO,^{23–26} it is apparent that the dominant series following excitation via a rotational level N' of the intermediate A state will be $np(N')$ and $nf(N'+2)$. Although from the angular momentum character of the A state one would expect to excite the $np(N')$ series predominantly, there is a much stronger transition dipole moment from the d character of the A state to the f Rydberg series, than there is from the s character of the A state to the p Rydberg series.²³ In Fig. 3 we present a frequency-resolved spectrum of autoionizing Rydberg states excited via the $A^2\Sigma^+(v'=2, N'=1, J'=3/2)$ intermediate in NO, and the spectrum is indeed dominated by the $np(1)$ and $nf(3)$ Rydberg series. The unperturbed positions of these Rydberg states are calculated using the Rydberg formula, taking Hund's case (d) quantum defects determined from high-resolution spectra $\mu_{p(1)}=0.7038$ and $\mu_{f(3)}=0.021$,²⁶ and marked with combs. It is worth mentioning that $np(3)$, $nf(1)$, $nd(2)$, and $ns(2)$ Rydberg series are also observed in this region of the spectrum. Around $\bar{n}_1=25, 30$, and 34 , there are near degeneracies between the $np(1)$ and $nf(3)$

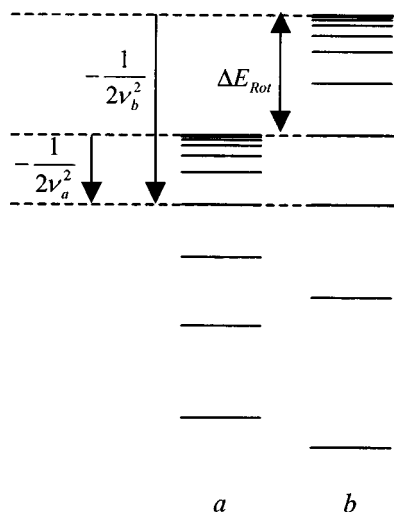


FIG. 4. A schematic energy level diagram illustrating the excitation of two Rydberg series (a) and (b) converging to two ionization limits separated by ΔE_{Rot} .

series. In the vicinities of these overlaps the overall line spacing is that of a single Rydberg series, whereas away from these regions the spectrum is more complicated. This is quite obviously the stroboscopic effect, at least visually, but it involves two series with different orbital angular momentum, unlike Na_2 . This is an important difference because the picture of an orbiting electron with an average principal quantum number coming into resonance with a rotating core is no longer valid. It is therefore necessary to develop a different physical explanation of the plateaus in the time-resolved spectra. With hindsight, a similar effect can also be observed in the frequency spectrum excited via the $A^2\Sigma^+(v'=1, N'=0, J'=1/2)$ intermediate in NO recorded by Goodgame *et al.* in Fig. 4(b) of Ref. 23 around $76\,940\text{ cm}^{-1}$, corresponding to the degeneracy between $30p(0)$ and $28f(2)$. Note that this also corresponds to the position of the plateaus observed in Fig. 1. Fredin *et al.* mention a fringe structure in the *s* and *d* Rydberg series of NO, but it is described as an “accident” arising from the phase of the *s*–*d* mixing and was specifically not of the same origin as the stroboscopic fringes observed in Na_2 .²⁴

Previous discussions of the stroboscopic effect have unfortunately neglected the influence of the quantum defect, although it obviously controls where the degeneracies between two series occur. We determine where the energy levels of two Rydberg series will overlap and include the effect of the quantum defect explicitly. Consider exciting two Rydberg series (a) and (b) converging to two separate ionization limits separated by ΔE_{Rot} (Fig. 4). There will be pairs of effective principal quantum numbers v_a and v_b , for which

$$\Delta E_{\text{Rot}} = \frac{1}{2v_b^2} - \frac{1}{2v_a^2} = \frac{(v_a + v_b)(v_a - v_b)}{2v_a^2 v_b^2} \approx \frac{(v_a - v_b)}{v_s^3}, \quad (3)$$

where $v_s = \sqrt{v_a v_b} \approx (v_a + v_b)/2$ is defined as the stroboscopic effective principal quantum number. This is valid for $2v_a^2 \Delta E_{\text{Rot}} \ll 1$. Rewriting $v_i = n_i - \mu_i$ and recognizing that $n_a - n_b = k$ is an integer, gives

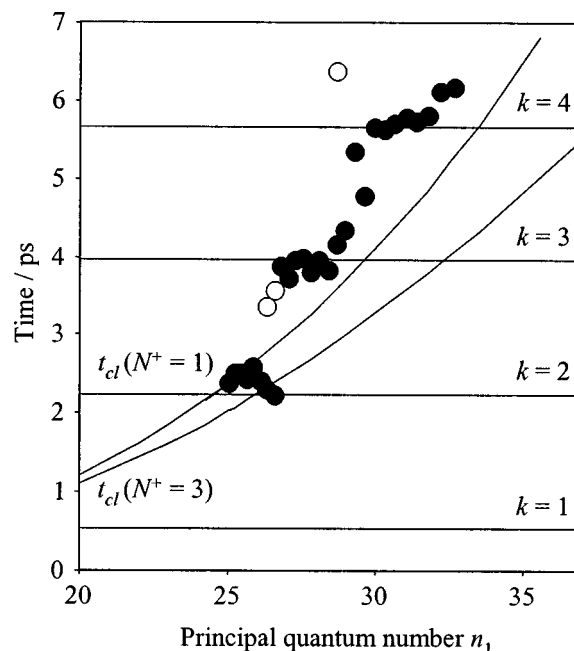


FIG. 5. A plot of the measured orbit period as a function of average excitation energy, expressed in terms of the average principal quantum number \bar{n}_1 , in the superposition. The wave packets are composed predominantly of $np(1)$ and $nf(3)$ Rydberg states with $v^+=2$. The trend lines mark the hydrogenic orbit periods and the solid horizontal lines mark the stroboscopic periods defined by Eq. (5).

$$\Delta E_{\text{Rot}} = (k + \Delta\mu)/v_s^3, \quad (4)$$

where $\Delta\mu = \mu_b - \mu_a$ is the difference in quantum defect between the two series. Equation (4) may then be rewritten in terms of the rotational beat period $T_{\text{Rot}} = 2\pi/\Delta E_{\text{Rot}}$, and stroboscopic period $T_s = 2\pi v_s^3$

$$T_s = T_{\text{Rot}}(k + \Delta\mu). \quad (5)$$

For the $np(0)$ and $nf(2)$ series in NO, the quantum defects determined experimentally are $\mu_{p(0)} = 0.7286$ and $\mu_{f(2)} = 0.0101$,²⁶ and the rotational beat period ($v^+=1$) is $T_{\text{Rot}} = 2.82$ ps. The stroboscopic periods may be calculated using Eq. (5) and are 0.79 ps ($k=1$), 3.61 ps ($k=2$), and 6.43 ps ($k=3$). These periods are represented in Fig. 1 as solid horizontal lines, and it is clear that the $k=3$ line passes straight through the most intense experimentally measured peaks in the recurrence spectra.

Figure 5 represents another example of the stroboscopic effect observed in wave packet spectra recorded following excitation of predominantly $np(1)$ and $nf(3)$ series via the $v'=2, N'=1, J'=3/2$ level of the *A* state. In this example, $B_2 = 1.950\text{ cm}^{-1}$, the rotational beat period $T_{\text{Rot}} = 1.71$ ps, and the quantum defect difference $\Delta\mu = 0.6328$.²⁶ Using Eq. (5) the stroboscopic periods are calculated to be 0.54 ps ($k=1$), 2.25 ps ($k=2$), 3.96 ps ($k=3$), and 5.67 ps ($k=4$). The experimentally measured data points form three very clear plateaus corresponding to the calculated stroboscopic periods for $k=2, 3$, and 4. These results (Figs. 1 and 5) demonstrate that the measured periods of motion in our system of two uncoupled Rydberg series, with different orbital angular momenta and rotational angular momenta, are separated by the rotational beat period, but they are shifted from

the rotational beat period by $\Delta\mu T_{\text{Rot}}$. Previous explanations of the stroboscopic effect defined $T_s = kT_{\text{Rot}}$ [from rearranging Eq. (1)] and neglected the influence of the quantum defect.

This shift introduced by the quantum defect can be explained if we treat the system as two separate Rydberg wave packets orbiting around different rotational states of the ion core. We start by modeling the plateaus in plots of recurrence time as a function of excitation energy, by calculating the autocorrelation function of a wave packet composed of two uncoupled Rydberg series (a) and (b) converging to two separate ionization limits separated by ΔE_{Rot} , as in Fig. 4. The autocorrelation function is written

$$|\langle \Psi(t) | \Psi(0) \rangle| = \left| \sum_{n=n_a, n_b} a_n^2 \exp(-i\omega_n t) \right|, \quad (6)$$

where

$$\Psi(r, t) = \sum_{n=n_a, n_b} a_n \psi_n(r) \exp(-i\omega_n t). \quad (7)$$

$\Psi(0)$ is the wave packet created at time $t=0$ which has evolved for time t when the second wave packet $\Psi(t)$ is created. In the calculation a number of simplifications are made. First, the energy levels are calculated using the Rydberg formula and assuming Hund's case (d) quantum defects μ_a and μ_b . Second, the population coefficients in the dipole approximation are calculated using $a_n = \langle \psi_n | r | \psi_{1s} \rangle \times \exp(-2 \ln 2 (E_n - \bar{E})^2 / \Delta E^2)$, where ΔE is the FWHM of the laser pulse, \bar{E} is its central frequency, and $\langle \psi_n | r | \psi_{1s} \rangle$ is calculated using hydrogenic wave functions. Finally, we make a weak-field approximation in which there is no depletion of the lower state and no ionization. Note that we use $1s$ ground-state wave functions because this is a model of a general system, rather than of NO specifically. Figure 6 plots the position of the first peak in the autocorrelation function calculated using Eq. (5), assuming a bandwidth $\Delta E = 21 \text{ cm}^{-1}$, a value of $\Delta E_{\text{Rot}} = 12 \text{ cm}^{-1}$, and quantum defects $\mu_a = 0$ and $\mu_b = 0, 0.2, 0.4, 0.6, 0.8$ (filled circles, triangles, squares, open circles, and crosses, respectively). Solid horizontal lines are drawn at times kT_{Rot} . It is clear from this figure that the calculated recurrence times for a given value of μ_b lie on a series of plateaus separated by the rotational beat period T_{Rot} , but shifted from kT_{Rot} by $\mu_b T_{\text{Rot}}$, i.e., they satisfy Eq. (5). The plateaus are quite flat at high n where the wave packet is composed of many Rydberg states and is well localized.

A. The role of the quantum defect in determining the stroboscopic period

The influence of the quantum defect on the dynamics of a wave packet composed of two interleaved Rydberg series can be understood by expanding the energy term of the wave packet expressed in Eq. (7), in terms of Taylor's series

$$\omega_{n_a} = -\frac{1}{2\bar{n}_a^2} \left[1 - 2\frac{\delta n}{\bar{n}_a} + 3\left(\frac{\delta n}{\bar{n}_a}\right)^2 + \dots \right] \quad (8a)$$

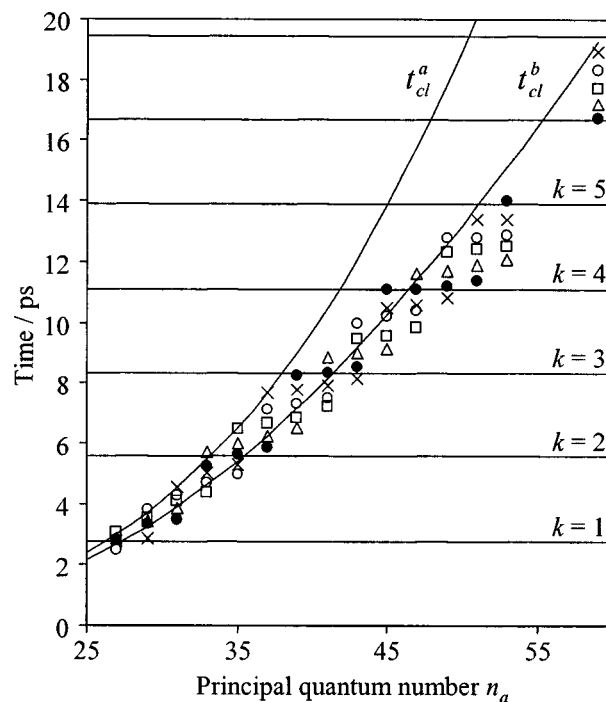


FIG. 6. A plot of the first peak in the autocorrelation function calculated using Eq. (6), assuming a bandwidth $\Delta E = 21 \text{ cm}^{-1}$, a value of $\Delta E_{\text{Rot}} = 12 \text{ cm}^{-1}$, and quantum defects $\mu_a = 0$ and $\mu_b = 0, 0.2, 0.4, 0.6, 0.8$ (filled circles, triangles, squares, open circles, and crosses, respectively). Solid horizontal lines are drawn at times kT_{Rot} .

$$\omega_{n_b} = -\frac{1}{2\bar{n}_b^2} \left[1 - 2\frac{\delta n}{\bar{n}_b} + 3\left(\frac{\delta n}{\bar{n}_b}\right)^2 + \dots \right] + \Delta E_{\text{Rot}}, \quad (8b)$$

where $\delta n = n - \bar{n}$. The first term in each expansion is the average energy of the wave packet in that series. The second terms are the harmonic frequencies and correspond to the classical periods, $t_{cl} = 2\pi\bar{n}^3$. Higher-order terms introduce dispersion effects, which are not required in this analysis. The quantum defect may be introduced in Eq. (8) by replacing the principal quantum number, n_i , with the effective principal quantum number, $v_i = n - \mu_i$ for Rydberg series i . The harmonic terms consequently gain a phase of

$$\exp\left(2\pi i \mu_i \frac{t}{t_{cl}}\right), \quad (9)$$

and the rotational energy of the core introduces a phase of

$$\exp\left(-2\pi i \frac{t}{T_{\text{Rot}}}\right), \quad (10)$$

where $T_{\text{Rot}} = 2\pi/\Delta E_{\text{Rot}}$ is the rotational beat period. For a peak to be observed in the Rydberg wave packet spectrum, electron wave packets in series (a) and (b) must both have returned to the core (i.e., $t \approx t_{cl}^a \approx t_{cl}^b$, which is true for $2v_a^2 \Delta E_{\text{Rot}} \ll 1$) and they must be in phase with one another, i.e., the phase difference between them must be $2\pi k$ (where k is an integer)

$$\left(\frac{\mu_a}{t_{cl}^a} - \frac{\mu_b}{t_{cl}^b} + \frac{1}{T_{\text{Rot}}}\right)t \approx \left(-\Delta\mu + \frac{t}{T_{\text{Rot}}}\right) = k. \quad (11)$$

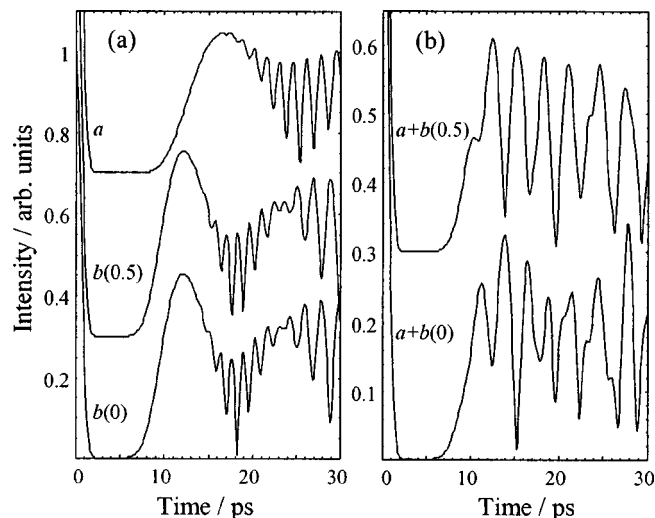


FIG. 7. Recurrence spectra calculated using Eq. (6), with $\Delta E = 21 \text{ cm}^{-1}$, $\Delta E_{\text{Rot}} = 12 \text{ cm}^{-1}$. The average principal quantum number in the excitation is $\bar{n}_a = 49$ (corresponding to $\bar{n}_b = 43.6$). In (a) time-resolved spectra of the individual wave packets are plotted for series *a* with quantum defect $\mu_a = 0$ (top trace), series *b* with $\mu_b = 0$ (bottom trace), and series *b* with $\mu_b = 0.5$ (middle trace). In (b), time-resolved spectra of the combined Rydberg series are plotted for $\mu_a = 0$ and $\mu_b = 0$ (bottom trace) and $\mu_b = 0.5$ (upper trace).

Equation (11) can be used in its precise form (the first set of brackets), or its approximate form (the second set of brackets). Recognizing that $t = T_s$ and rearranging the approximate form of Eq. (11) yields the expression for the stroboscopic period expressed earlier as Eq. (5). The physical interpretation is as follows: Two independent wave packets are launched in one molecule; each wave packet follows its own trajectory (different angular momentum and different average principal quantum number) around a core with well-defined rotational angular momentum. Each wave packet acquires its own phase from both the rotation of the molecular core and the electronic quantum defect. When the two wave packets overlap spatially they interfere, and the interference pattern depends on the phase relationship between them. When the wave packets are in phase they interfere constructively and the Rydberg population is enhanced, and when they are out of phase they interfere destructively and the Rydberg population is depleted. Thus, the positions of peaks in the wave packet recurrence spectrum is dependent on the molecular phase which arises from the rotation of the core and the electronic phase which comes from the quantum defect.

The interference patterns generated by the periodic phase difference between two Rydberg series are illustrated well in the regime where $t_{cl} > T_{\text{Rot}}$ (Fig. 7). Recurrence spectra are calculated using Eq. (6), with the same assumptions as before ($\Delta E = 21 \text{ cm}^{-1}$ and $\Delta E_{\text{Rot}} = 12 \text{ cm}^{-1}$) and quantum defects $\mu_a = 0$, and $\mu_b = 0$ or 0.5 . The average principal quantum number in the excitation is $\bar{n}_a = 49$ (corresponding to $\bar{n}_b = 43.6$). In Fig. 7(a) time-resolved spectra of the individual wave packets are plotted. The influence of the quantum defect is already apparent. Comparing the spectra for wave packets in series (b), with quantum defects $\mu_b = 0$ (bottom trace) and 0.5 (middle trace), the high-order partial re-

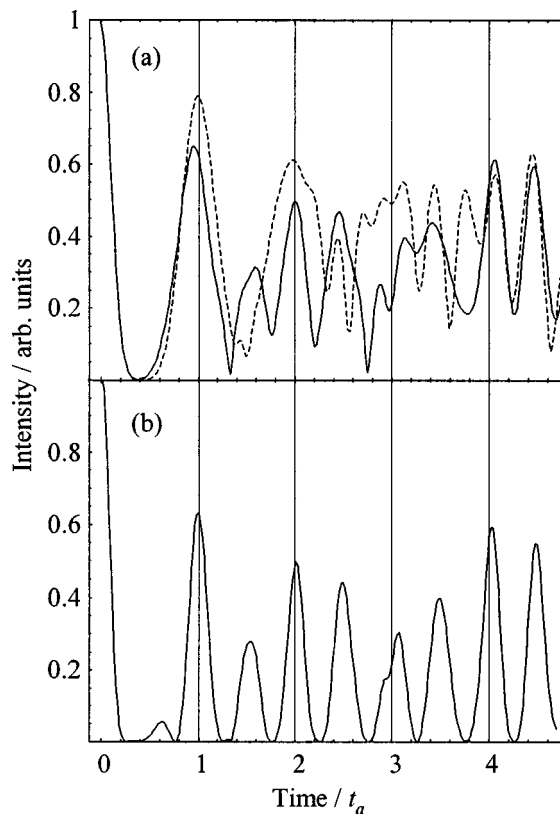


FIG. 8. (a) A recurrence spectrum, calculated using Eq. (6), with $\Delta E = 21 \text{ cm}^{-1}$, $\Delta E_{\text{Rot}} = 12 \text{ cm}^{-1}$, and quantum defects $\mu_a = \mu_b = 0$ (solid line). The excitation energy is chosen to satisfy the resonance condition $t_a = 2T_{\text{Rot}}$ ($\bar{n}_a = 33.2$). For comparison, a recurrence spectrum for a single Rydberg series with $\bar{n}_a = 33.2$ is calculated using the same parameters (dashed line). (b) A recurrence spectrum calculated for a single Rydberg series convoluted with the autocorrelation function of a rotating core, $1 + \cos(2\pi t/T_{\text{Rot}})$, with periods chosen to satisfy the resonance condition $t_a = 2T_{\text{Rot}}$.

vivals which appear after approximately 18 ps are exactly out of phase with one another. This is a well-known result: the first-order term in the Taylor's expansion leads to a temporal shift at the m th-order partial revival, $\delta t = t_{cl}\mu_i/m$.¹⁰ In Fig. 7(b), time-resolved spectra of the combined Rydberg series are plotted for $\mu_b = 0$ (bottom trace) and $\mu_b = 0.5$ (upper trace). When the wave packets return to the core they overlap spatially and generate interference patterns in the Rydberg electron population. These interference patterns are observed in the wave packet spectrum as fast oscillations at the rotational beat frequency. Adding a quantum defect of 0.5 to one of the Rydberg series shifts the fast oscillations by $T_{\text{Rot}}/2$. Interestingly, the interference of the two wave packets is analogous to Young's double slit experiment: The light emerging from the two slits in the original experiment is replaced by the two wave packets in the two Rydberg series, and the distance between the slits is analogous to the separation between the ionization limits of the two series.

An interesting situation arises in the special resonance condition

$$t_{cl} = 2T_{\text{Rot}}. \quad (12)$$

In Fig. 8(a) a recurrence spectrum is calculated using Eq. (6), with the same parameters as before ($\Delta E = 21 \text{ cm}^{-1}$ and

$\Delta E_{\text{Rot}} = 12 \text{ cm}^{-1}$) and quantum defects $\mu_a = \mu_b = 0$ (solid line). The excitation energy is chosen to satisfy Eq. (12) for Rydberg series (a). Specifically, $T_{\text{Rot}} = 2.8 \text{ ps}$ and $n_a = 33.2$ ($t_a = 5.6 \text{ ps}$), which corresponds to $n_b = 31.4$ ($t_b = 4.7 \text{ ps}$). Peaks are observed in the recurrence spectrum at multiples of the classical period t_a , when both the rotational and electronic motions are in phase with one another. Peaks are also observed at $(k + 0.5)t_{cl}$ where $k > 0$ is an integer, i.e., at odd multiples of the rotational beat period. At $(k \pm 0.25)t_{cl}$ minima are observed, i.e., at odd multiples of $T_{\text{Rot}}/2$ when the rotational beat is at a minimum. For comparison, a single wave packet spectrum with $n_a = 33.2$ is calculated (dashed line). It is particularly interesting to observe how the second wave packet interferes with the first, constructively at $(k + 0.5)t_{cl}$ in regions where there is low (but nonzero) electron density from the first wave packet, and destructively at $(k \pm 0.25)t_{cl}$ even in regions where there is significant electron density from the first wave packet. The two-series spectrum resembles the recurrence spectrum calculated using semiclassical methods, and described in Sec. I.²¹ In fact, it is possible to mimic the results of the semiclassical calculations using our wave packet calculation. In the limit of high n and high rotational quantum numbers, both the electronic motion and nuclear rotation are classical. In this limit, the rotational period given by Eq. (1) becomes equivalent to the rotational beat period. A reasonable model is to treat the autocorrelation functions of the electron wave packet and the rotating core separately and convolute the two spectra. For direct comparison, we use similar parameters as above ($\Delta E = 21 \text{ cm}^{-1}$ and $\Delta E_{\text{Rot}} = 12 \text{ cm}^{-1}$), but calculate the recurrence spectrum of a single Rydberg series with $n_a = 33.2$ ($\mu_a = 0$) and convolute it with the autocorrelation function of the rotating core, $1 + \cos(2\pi t/T_{\text{Rot}})$. $T_{\text{Rot}} = 2.8 \text{ ps}$ to satisfy the resonance condition Eq. (11). The result is plotted in Fig. 8(b) and it is similar to the two-series calculation represented in Fig. 8(a). The single-series calculation is valid for very high rotational quantum numbers and principal quantum numbers, and in fact, very closely resembles the recurrence spectrum calculated semiclassically, with $J = 50$ and $n = 8$ in Fig. 14 of Ref. 21.

IV. SUMMARY

In this paper we have investigated in detail the dynamics of Rydberg electron wave packets in a molecular system. Peaks in the autocorrelation function of a wave packet composed predominantly of two interleaved Rydberg series are observed at a stroboscopic period, which depends on both the difference in the ionization limits of the two series, and on the quantum defects. This observation has been rationalized by viewing the system as one in which two electron wave packets evolve independently until they overlap spatially. The resulting interference between the two wave packets determines the positions of maxima and minima in the electron probability distribution, and hence the times at which peaks are observed in the autocorrelation function. These interference patterns depend on the relative phases of the two wave packets, which in turn depend on the rotational energy of the molecular core and on the quantum defects.

The concept of phase in wave packet dynamics is very important, particularly in the field of coherent control. Knowledge of the sources of phase in a molecular system, and how it can be manipulated by optical phase, is crucial to the design of intuitive coherent control schemes, e.g., Refs. 27, 28. Because it is relatively simple to understand where the phase comes from in a Rydberg system, and because in a Rydberg molecule all the sources of molecular phase are present (molecular rotation and vibration), these systems make ideal laboratories for developing and testing new coherent control strategies, which may eventually be applied to larger, more complex molecular systems.

ACKNOWLEDGMENTS

We thank the EPSRC for equipment funding, postdoctoral funding (V.G.S.), and a studentship (R.A.L.S.). We also thank King's College London for a studentship (J.R.R.V.). We are grateful to P. Brint and A.L. Goodgame for their help in setting up the lasers in Oxford to record the frequency spectrum. We also thank J. R. Heine for one of the figures, and A. Stoliarov for useful discussions.

- ¹J. Parker and C. R. Stroud, Phys. Rev. Lett. **56**, 716 (1986).
- ²W. A. Henle, H. Ritsch, and P. Zoller, Phys. Rev. A **36**, 683 (1987).
- ³J. Grochmalicki and M. Lewenstein, J. Phys. B **21**, 3285 (1988).
- ⁴A. t. Wolde, L. D. Noordam, A. Lagendijk, and H. B. v. L. v. d. Heuvel, Phys. Rev. Lett. **61**, 2099 (1988).
- ⁵J. A. Yeazell, M. Mallalieu, J. Parker, and C. R. Stroud, Phys. Rev. A **40**, 5040 (1989).
- ⁶I. S. Averbukh and N. F. Perel'man, Sov. Phys. JETP **69**, 464 (1989).
- ⁷J. A. Yeazell and C. R. Stroud, Phys. Rev. A **43**, 5153 (1991).
- ⁸R. Bluhm and V. A. Kosteletzky, Phys. Rev. A **51**, 4767 (1995).
- ⁹R. Bluhm, V. A. Kosteletzky, and B. Tudose, Phys. At. Nucl. **61**, 1948 (1998).
- ¹⁰J. Wals, H. H. Fielding, and H. B. v. L. v. d. Heuvel, Phys. Scr. **T58**, 62 (1995).
- ¹¹R. A. L. Smith, J. R. R. Verlet, E. D. Boleat, V. G. Stavros, and H. H. Fielding, Faraday Discuss. **115**, 63 (2000).
- ¹²V. G. Stavros, J. A. Ramsell, R. A. L. Smith, J. R. R. Verlet, J. Lei, and H. H. Fielding, Phys. Rev. Lett. **83**, 2552 (1999).
- ¹³V. G. Stavros, J. A. Ramsell, R. A. L. Smith, J. R. R. Verlet, J. Lei, and H. H. Fielding, Phys. Rev. Lett. **84**, 1847 (2000).
- ¹⁴S. Martin, J. Chevalere, M. C. Bordas, S. Valignat, M. Broyer, B. Cabaud, and A. Hoareau, J. Chem. Phys. **79**, 4132 (1983).
- ¹⁵C. H. Greene and C. Jungen, Adv. At. Mol. Phys. **21**, 51 (1985).
- ¹⁶P. Labastie, C. Bordas, B. Tribollet, and M. Broyer, Phys. Rev. Lett. **52**, 1681 (1984).
- ¹⁷D. Gauyacq, A. L. Roche, M. Seaver, S. D. Coulson, and W. A. Chupka, Mol. Phys. **71**, 1311 (1990).
- ¹⁸M. Lombardi, P. Labastie, M. C. Bordas, and M. Broyer, J. Chem. Phys. **89**, 3479 (1988).
- ¹⁹C. Tsai, J. Bahns, and W. C. Stwalley, Chem. Phys. Lett. **236**, 553 (1995).
- ²⁰E. S. Chang, J. Li, J. Zhang, C. Tsai, J. Bahns, and W. C. Stwalley, J. Chem. Phys. **111**, 6247 (1999).
- ²¹S. N. Altunata, J. Cao, and R. W. Field, Phys. Rev. A **65**, 053415 (2002).
- ²²L. D. Noordam, D. I. Duncan, and T. F. Gallagher, Phys. Rev. A **45**, 4734 (1992).
- ²³A. L. Goodgame, H. Dickinson, S. R. Mackenzie, and T. P. Softley, J. Chem. Phys. **116**, 4922 (2002).
- ²⁴S. Fredin, D. Gauyacq, M. Horani, C. Jungen, and G. Lefevre, Mol. Phys. **60**, 825 (1987).
- ²⁵M. J. J. Vrakking, J. Chem. Phys. **105**, 7336 (1996).
- ²⁶M. J. J. Vrakking and Y. T. Lee, J. Chem. Phys. **102**, 8818 (1995).
- ²⁷J. R. R. Verlet, V. G. Stavros, and H. H. Fielding, Phys. Rev. A **65**, 032504 (2002).
- ²⁸J. R. R. Verlet, V. G. Stavros, R. S. Minns, and H. H. Fielding, Phys. Rev. Lett. **89**, 263004 (2002).